COMPLEX FRANK LOOPS AND FAULT CLIMB

By A. J. Morton* and L. M. Clarebrough*

[*Manuscript received December* 19, 1968]

Summary

The Burgers vectors of the dislocations bounding steps in the stacking fault in Frank dislocation loops in quenched silver and copper–aluminium alloys have been identified by comparison of experimental electron microscope images and images computed using the Head–Humble technique. The steps in the fault are generally acute, faulted, and bordered by $\frac{1}{6}\langle 110\rangle$ stair-rod dislocations. However, obtuse unfaulted steps bordered by $\frac{1}{6}\langle 112\rangle$ Shockley dislocations have also been observed. A characteristic configuration for a stepped loop consists of a triangular region within the main loop with one edge, a dissociated Frank dislocation, forming an edge of the main loop, and the other two edges, acute fault bends bordered by $\frac{1}{6}\langle 110\rangle$ dislocations, forming steps in the fault.

The formation of steps may occur by the union of separate loops involving dissociation of parallel edges on a common $\{111\}$ plane. However, the formation of the triangular configuration and of steps bordered by $\frac{1}{6}\langle 112\rangle$ dislocations is not compatible with this mechanism. An alternative mechanism, fault climb, is compatible with all observations. It is concluded that vacancy supersaturation is reduced in quenched materials of low stacking fault energy by fault climb, the formation of steps in the fault resulting from climb up and climb down in different portions of a loop.

I. Introduction

In an investigation into the nature of faulted defects in quenched silver, Clarebrough, Segall, and Loretto (1966) observed complex defects consisting of Frank dislocation loops containing steps in the stacking fault. In quenched aluminium, faulted Frank dislocation loops are common and intensive investigations have revealed the presence of multilayer Frank dislocation loops with two, three, and four faulted planes in close proximity (cf. for example, Edington and West 1966). However, complex defects of the type observed in silver have not been reported for aluminium. Since the stacking fault energy of silver is much lower than that of aluminium, it is likely that the formation of stepped faulted loops is associated with low stacking fault energy.

This paper reports a study of complex Frank loops in quenched specimens of pure silver and copper–aluminium alloys. For several defects, the dislocation arrangement at the fault bends has been determined by a comparison of computed and experimental images. It is shown that in some cases the Burgers vectors of the dislocations at the steps are compatible only with the formation of the steps by climb of the stacking fault.

* Division of Tribophysics, CSIRO, University of Melbourne, Parkville, Vic. 3052.

II. Experimental

The silver and copper–aluminium alloys used in this investigation were the same as used previously (Clarebrough and Morton 1969*b*), as were the methods of determining the sense of the reflecting vector and the planes of the faulted loops. The nature of the stacking fault was determined from bright field images of loops which intersected a foil surface. From the nature of the outermost fringe the value of $\boldsymbol{g}.\boldsymbol{R}$ is fixed (Hashimoto, Howie, and Whelan 1962) so that the known $\boldsymbol{g}$ determines $\boldsymbol{R}$. In all cases examined, the faults were intrinsic.

III. General Observations

For the quenching conditions used in these experiments, the Frank loops in both silver and the copper–aluminium alloys were generally large, loops with edge lengths of approximately $0 \cdot 5\,\mu$ were common, and occasionally loops with edge lengths of approximately $1\,\mu$ were observed. The loops always had edges along $\langle 110\rangle$ directions, but regular hexagonal loops were rare. The density of loops was very variable, no loops being observed in some foils. The maximum density of loops in both silver and the copper–aluminium alloys was approximately 5×10^{13} cm^{-3} and in regions with this density 25% of the loops were usually complex. For faster quenching rates, regions with a density of loops of 10^{14} cm^{-3} were common and a higher percentage of the loops appeared to be complex. However, for fast quenching rates the complex loops were too small for detailed analysis.

It is readily shown that a complex loop involves a step in a single stacking fault if the step is large, by observing an offset when the main part of the loop is on a vertical plane or by rotating the specimen so that the step is clearly resolved. An example of a large step in a loop in the copper–aluminium (9·4%) alloy is shown in Figure 1. In Figure 1(*a*) the loops are viewed in the [057] beam direction. Loop 1 is a simple Frank loop on (111), whilst loop 2, on $(\bar{1}11)$, intersects the bottom of the foil along ACB and is complex with a step along [101] (CD). The fringe shift at the step, which is on $(11\bar{1})$, suggests that the step height is approximately one extinction distance for a 200 reflection. Since the step is on a plane that is nearly vertical in Figure 1(*a*), it cannot be seen clearly. In Figure 1(*b*) the beam direction is [103] and the step can be seen to be faulted. In Figure 1(*c*) the beam direction is [213] and the plane of the step is again vertical, so that no fault contrast is observed.

The large step shown in Figure 1 is an exceptional case and usually steps were detected by contrast effects along $\langle 110\rangle$ directions within the loop. For 020 and 111 reflections, a step was usually detected by a displacement of the fault fringes in the loop on crossing the step and often contrast along the $\langle 110\rangle$ direction of the step was associated with the fringe displacement. An example of strong contrast for a 111 reflection at the interior edges of a triangular region in a large loop in silver is shown in Figure 3(*a*). The observed features of the contrast along steps for 020 and 111 reflections were more complex than the dark contrast for 111 reflections and the light contrast for 020 reflections analysed by Tunstall and Goodhew (1966) for overlapping Frank loops in aluminium. For 220 or 311 reflections, for which the fault in the loop was out of contrast, contrast was usually observed along the $\langle 110\rangle$ direction associated with the step. In most cases, for 220 reflecting vectors

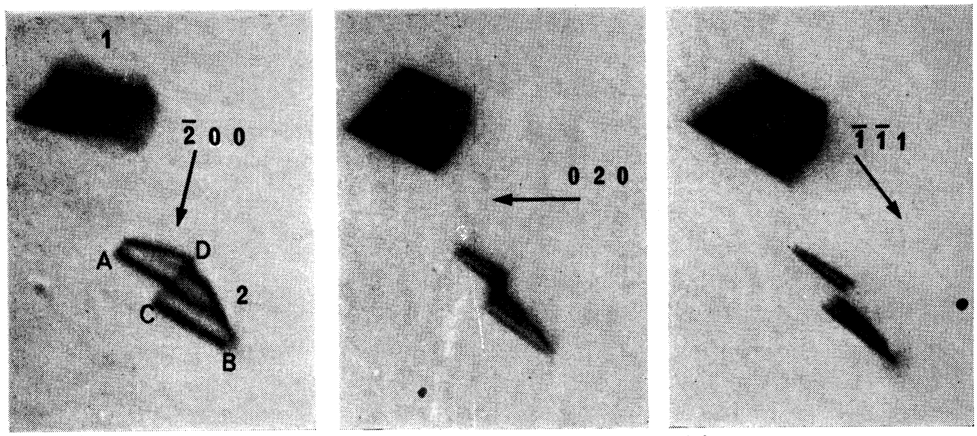

1(*a*) 1(*b*) 1(*c*)

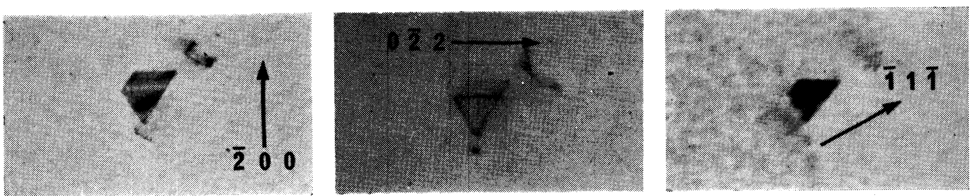

2(*a*) 2(*b*) 2(*c*)

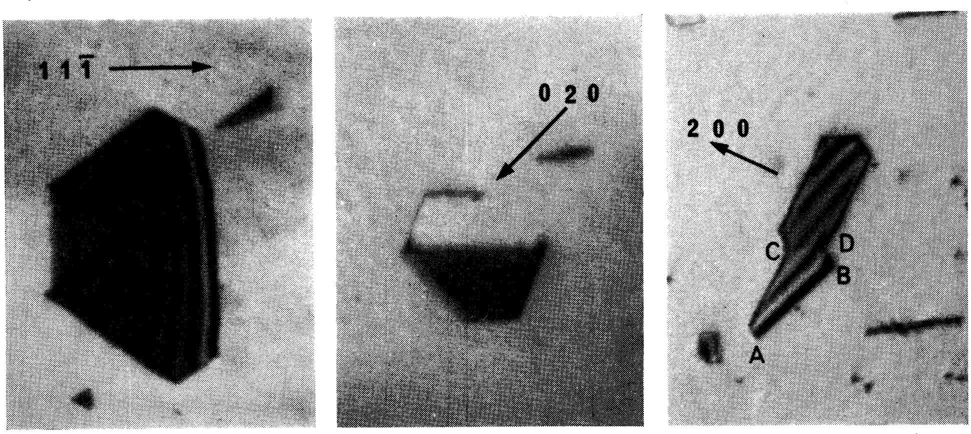

3(*a*) 3(*b*) 3(*c*)

Fig. 1.—Complex loop in a copper–aluminium (9·4 at.%) alloy ($\times$120 000). The electron beam directions are (*a*) [057], (*b*) [103], and (*c*) [213]. The operative reflections are indicated.

Fig. 2.—Complex loop in a copper–aluminium (9·4 at.%) alloy ($\times$60 000). The electron beam directions are (*a*) [057], (*b*) [$\bar{1}$56], and (*c*) [$\bar{1}$55]. The operative reflections are indicated.

Fig. 3.—Complex loops in silver and a copper–aluminium (9·4 at.%) alloy ($\times$60 000): (*a*) silver, beam direction [112]; (*b*) silver, [102]; (*c*) copper–aluminium, [011]. The operative reflections are indicated.

parallel to the ⟨110⟩ direction of the step, contrast was not observed, indicating that the steps were bounded by edge dislocations.* However, two examples were found where strong contrast was observed for a 220 diffracting vector parallel to the ⟨110⟩ direction of the step, and one of these is shown in Figure 2. Details of the observed contrast are given in Section V where it will be shown from a comparison of experimental and computed images that the contrast effects arise from steps in the stacking fault.

The unfaulting behaviour of the complex loops is compatible with steps in a stacking fault. In many cases unfaulting was observed to occur up to the ⟨110⟩ direction across the loop, associated with a step, before the whole loop unfaulted. Thus the first stage of unfaulting left a loop with a Frank dislocation bounding a faulted region on one side of the step and a prismatic dislocation bounding an unfaulted region on the other side (Fig. 3(*b*)). For the example of unfaulting in Figure 3(*b*), the loop is on $(1\bar{1}1)$ and portion of the prismatic dislocation which was along $[\bar{1}01]$ has slipped out of the foil on (111).

Only one example was found where the shape of the defect suggested that the step arose from the combination of two separate Frank loops. The shape of the defect in Figure 3(*c*) suggests that the step along CD arose from two closely spaced loops on (111) (one of the loops intersects the surface along AB) combining along $[\bar{1}01]$ (CD) by dissociation on $(1\bar{1}1)$.

Specimens of quenched aluminium were examined for the presence of stepped loops but none were observed. It is concluded that if stepped loops form in quenched aluminium their concentration must be several orders of magnitude less than in silver and the copper–aluminium alloys.

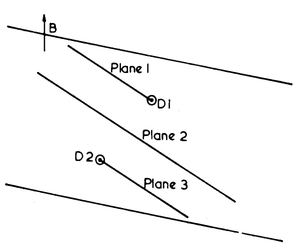

Fig. 4.—Geometrical arrangement of fault planes and dislocations used in image computation for overlapping Frank dislocation loops.

IV. Image Computation

Computation of contrast, arising from particular dislocation configurations that may be involved at the steps in complex loops, has been carried out using the technique of Head (1967), but with the extended programme of Humble (1968) which enables the treatment of two parallel dislocations bounding up to three faulted planes in a foil of arbitrary orientation. The values of elastic constants, anomalous and real absorption constants, and extinction distance used here are as given previously (Clarebrough and Morton 1969*a*, 1969*b*). Variation in the visibility limits from 7% below and 15% above background intensity is indicated in the figure captions.

In order to consider the possibility that the observed contrast in complex loops may arise from overlapping Frank loops, a modification was made to the computer

* This conclusion remains valid for anisotropic materials (Head, Loretto, and Humble 1967).

programme to treat situations similar to that shown in Figure 4. Here plane 2 is always parallel to plane 1 and extends over all fields of the computed image. Plane 2 no longer is bounded by dislocations 1 and 2, but does contain the dislocation direction. With plane 3 and dislocation 2 absent, the geometry then reduces to overlapping faulted planes with one plane terminating in the field of the micrograph.

V. Comparison of Experimental and Computed Images

A large number of possibilities exist for the Burgers vectors of the dislocations bordering a step in a complex loop. These cases can be reduced to a large extent by excluding the possibility of extrinsic faulting in the step in the present experiments.* Burgers vectors for stair-rod dislocations that may be present along $[\bar{1}10]$ for a step on $(11\bar{1})$ in a fault on (111) are given in Table 1. Dislocations with Burgers vectors greater than $\frac{1}{6}\langle 301\rangle$ are probably unstable (Friedel 1955) and have not been considered. The choices available in Table 1 can be reduced by knowing if the bend in the fault is acute or obtuse and if the dislocations bordering the step are of edge orientation. In addition to the stair-rod dislocations of Table 1, the possibility of an unfaulted step bordered by Shockley or Frank dislocations must be considered.

Table 1

Burgers vectors for intrinsic fault bends along $[\bar{1}10]$

Burgers vector	$\frac{1}{6}[\bar{1}\bar{1}0]$	$\frac{1}{3}[110]$	$\frac{1}{3}[001]$	$\frac{1}{6}[30\bar{1}]$	$\frac{1}{6}[03\bar{1}]$	$\frac{1}{6}[0\bar{3}\bar{1}]$	$\frac{1}{6}[\bar{3}0\bar{1}]$
Bend	Acute	Acute	Obtuse	Obtuse	Obtuse	Obtuse	Obtuse

The angle of the fault bend at the step can sometimes be determined from projections of the defect in different beam directions and sometimes from the sense of the fringe shift at the step for loops that intersect the foil surface, or by matching the intensities of fringes across the step in a loop that does not intersect the surface. Whether the dislocations are of edge orientation can be determined by using the reflecting vector parallel to the $\langle 110\rangle$ direction of the step edge. Usually either the nature of the bend or the character of the dislocations could be determined, but in some instances neither of these variables was known.

Comparisons between experimental and computed images have been made for silver and the copper–aluminium (9·4%) alloy.

A very characteristic configuration for complex loops in silver and copper–aluminium alloys is a triangular region within the main loop with one edge of the triangular region along one edge of the loop.

A complex loop of this form in silver is shown in Figure 5 for various reflecting vectors and beam directions. The loop lies on (111) and the region EFG is bounded by directions $[10\bar{1}]$ (EF), $[0\bar{1}1]$ (FG), and $[\bar{1}10]$ (GE).

* Although the formation of extrinsic faults is unlikely, for each case considered in this section the appropriate Burgers vectors for intrinsic–extrinsic fault bends were tested by image computations. In no case were the computed images of intrinsic–extrinsic combinations compatible with the experimental images.

5(*a*)

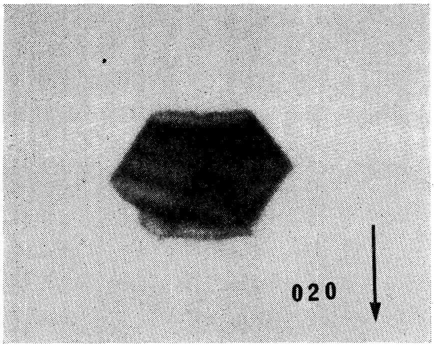

5(*b*)

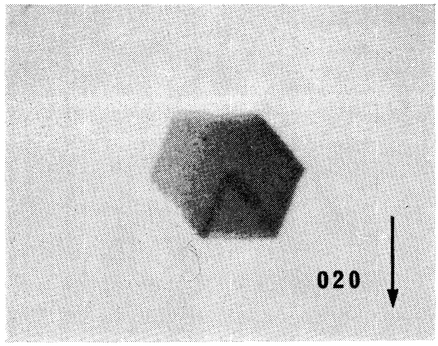

5(*c*)

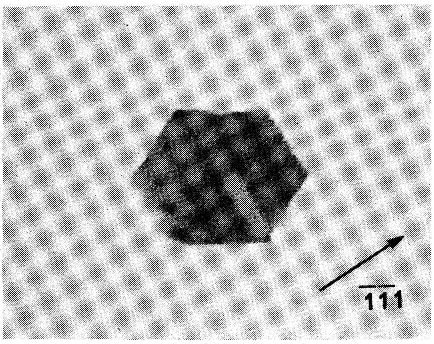

5(*d*)

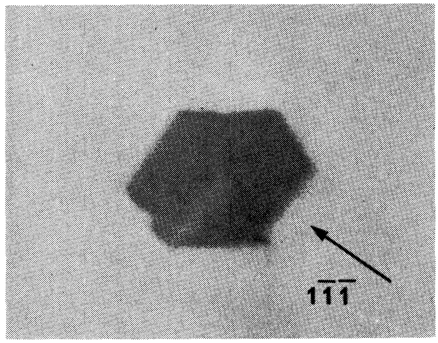

5(*e*)

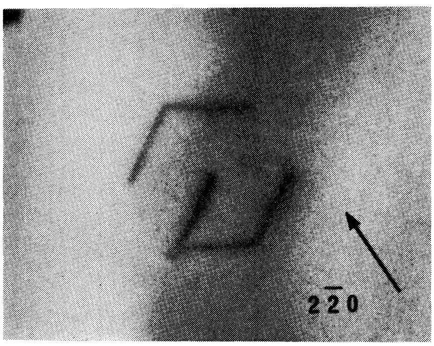

5(*f*)

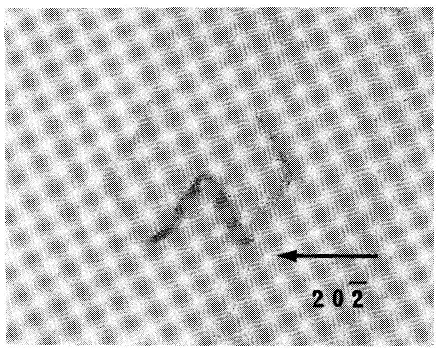

5(*g*)

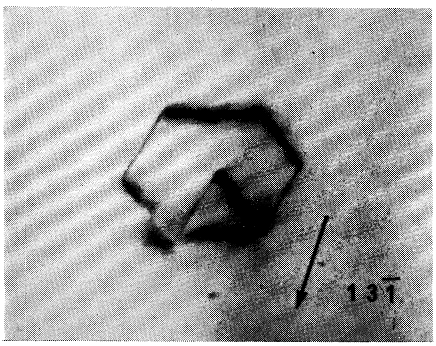

5(*h*)

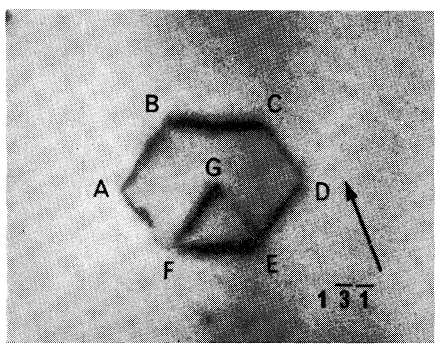

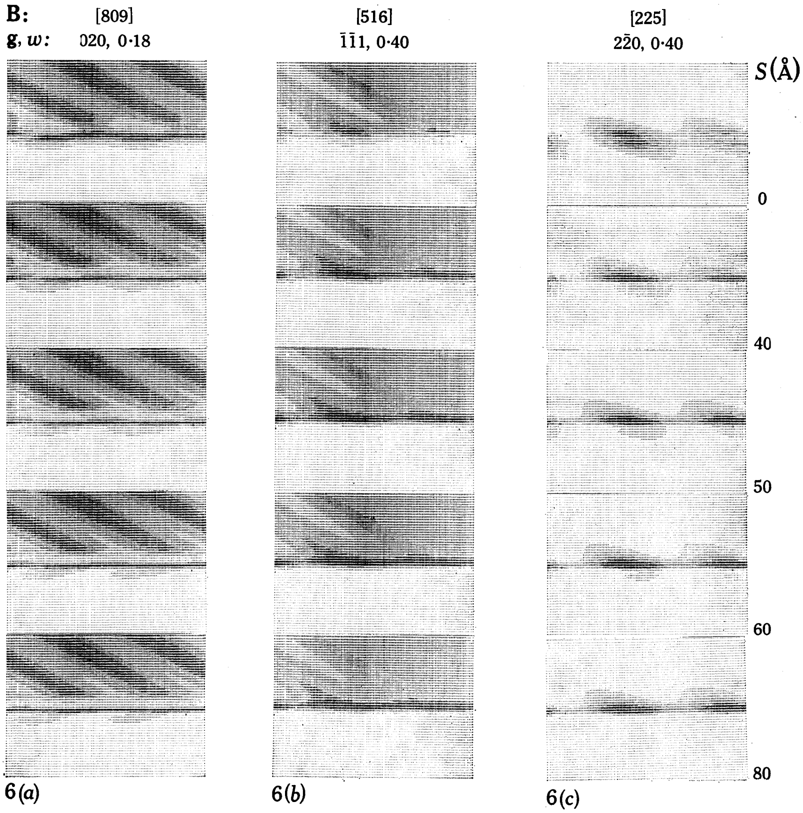

Fig. 6 (*above*).—Computed images of undissociated and dissociated Frank dislocations along the edge FE of the Frank loop shown in Figure 5:

$$\boldsymbol{FN}\ [418], \qquad \boldsymbol{u}\ [\bar{1}01], \qquad t = 9\xi_{111}.$$

The values of S, $\boldsymbol{B}$, $\boldsymbol{g}$, and w are indicated. Line resolution is 23 Å.

Fig. 5 (*opposite*).—Complex Frank dislocation loop in quenched silver ($\times$100 000):

(*a*) $\boldsymbol{B}$ [809], $\boldsymbol{g}$ 020; (*b*) $\boldsymbol{B}$ [103], $\boldsymbol{g}$ 020;
(*c*) $\boldsymbol{B}$ [516], $\boldsymbol{g}$ $\bar{1}\bar{1}1$; (*d*) $\boldsymbol{B}$ [817], $\boldsymbol{g}$ $1\bar{1}\bar{1}$;
(*e*) $\boldsymbol{B}$ [225], $\boldsymbol{g}$ $2\bar{2}0$; (*f*) $\boldsymbol{B}$ [515], $\boldsymbol{g}$ $20\bar{2}$;
(*g*) $\boldsymbol{B}$ [518], $\boldsymbol{g}$ $13\bar{1}$; (*h*) $\boldsymbol{B}$ [$5\bar{1}8$], $\boldsymbol{g}$ $1\bar{3}\bar{1}$.

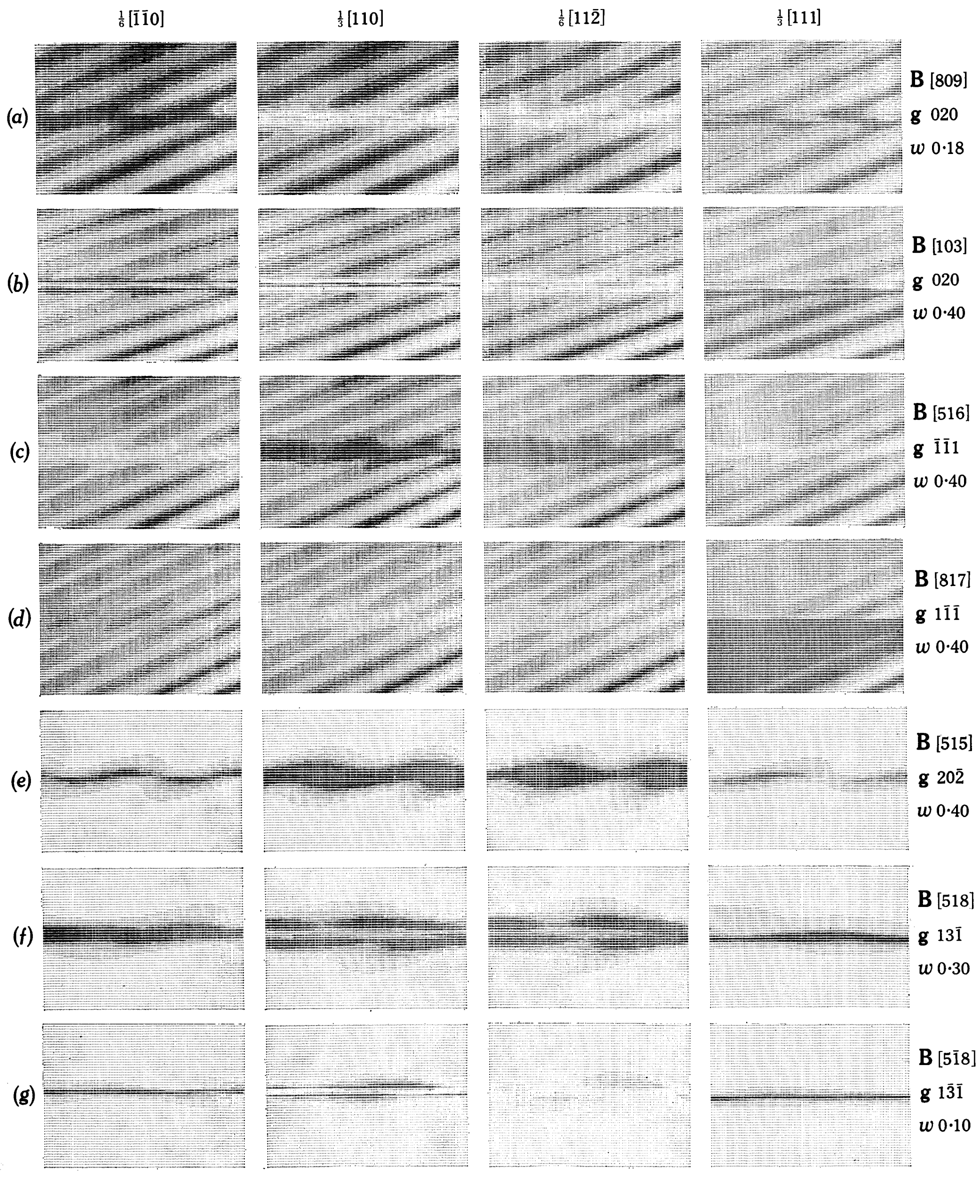

Fig. 7.—Computed images of the step EG in the complex Frank dislocation loop shown in Figure 5 for different Burgers vectors of the dislocations at the step edge and for various reflecting vectors:

$$S = 180\ \text{Å}, \qquad \boldsymbol{FN}\ [418], \qquad \boldsymbol{u}\ [1\bar{1}0] \qquad t = 9\xi_{111}.$$

The Burgers vectors and the values of $\boldsymbol{B}$, $\boldsymbol{g}$, and w are indicated. Line resolution is 30 Å in (*a*)–(*d*), 20 Å in (*e*), and 40 Å in (*f*) and (*g*).

It is clear from the images for the $13\bar{1}$ and $1\bar{3}\bar{1}$ reflections (Figs 5(*g*) and 5(*h*)) that the loop does not intersect either foil surface. Further, from the obvious protrusion outside the main loop of the projection of the triangular region in Figures 5(*c*) and 5(*d*), it is apparent that a large separation exists between the triangular region and the main loop. For the $2\bar{2}0$ and $20\bar{2}$ reflections, there is no contrast along GE and EF respectively, showing that the dislocations along these directions are of pure edge character. It should be noted that for both the $2\bar{2}0$ and $20\bar{2}$ reflections the edges of the hexagonal loop show the contrast typical of dissociated Frank dislocations (Clarebrough and Morton 1969*a*) in that the images are continuous dark lines where $\boldsymbol{g}$ is not parallel to $\boldsymbol{u}$.

The characteristic feature of the images obtained for the 020 reflection is that for the [809] beam direction (Fig. 5(*a*)) there is a broad dark line of contrast along both FG and GE (cf. Fig. 5(*h*)), whereas for [103] (Fig. 5(*b*)) the contrast along GE is resolved into two fine dark lines approximately 100 Å apart, but the contrast for the edge FG remains single. The contrast at the outer edge EF also varies on rotating from [809] to [103], the light band visible in [809] inside the line of contrast along EF becoming narrower in the [103] beam direction. The similarity in contrast for edges BC and EF for the 020 and all other reflections should be noted.

For the $\bar{1}\bar{1}1$ reflection, the contrast along EF is similar to that for the $1\bar{1}\bar{1}$ reflection. However, the contrast for edges GE and FG interchange for these two reflections; the light band along GE for the $\bar{1}\bar{1}1$ reflection fading into the general fault contrast for $1\bar{1}\bar{1}$, and the contrast along FG for $\bar{1}\bar{1}1$ becoming a broad light band for the $1\bar{1}\bar{1}$ reflection. The similar contrast along FG and GE for the 111 reflection normal to the dislocation line suggests a similar arrangement of dislocations and faults along these directions.

The contrast along GE is a strong dark line for the $13\bar{1}$ reflection, but is weak for the $1\bar{3}\bar{1}$, whereas for the edge FG the contrast is strong for $1\bar{3}\bar{1}$ and consists of a fine dark line (40 Å wide) for the $13\bar{1}$ reflection. For both the $13\bar{1}$ and $1\bar{3}\bar{1}$ reflections there is a strong dark line of contrast along FE.

From the general observations of contrast in the experimental images, it is possible to eliminate many of the possible dislocation configurations. The protrusion of the triangular region requires that if faulted steps exist along FG and GE they must be acute steps. Secondly, the lack of contrast along GE for the 220 reflection and along EF for the $20\bar{2}$ reflection requires that dislocations of edge character bound the region along these directions.

Since an image for the $0\bar{2}2$ reflection was not obtained, no conclusion could be drawn about the character of the dislocations along FG. For this reason the dislocation configurations at the edges EF and GE will be considered first.

It was noted above that the contrast along edges BC and EF was similar for all reflecting vectors, suggesting that the dislocations along BC and EF have the same Burgers vector. Computations of the contrast from both undissociated and dissociated Frank dislocations along EF for the 020, $\bar{1}\bar{1}1$, and $2\bar{2}0$ reflections are given in Figure 6 for various separations of Shockley and stair-rod dislocations. Matching of experimental and computed images indicates that the dislocation along EF is a dissociated Frank dislocation with a separation of the Shockley and stair-rod dislocations of approximately 60 Å.

Of the possible dislocation and fault configurations for the edge GE, only four satisfy the above observations. If the step is faulted, the Burgers vector of the stair-rod dislocation dipole at the step edge must be either $\frac{1}{6}[\bar{1}\bar{1}0]$ or $\frac{1}{3}[110]$ and if no fault is present on the step, the dislocation may be a $\frac{1}{6}[11\bar{2}]$ Shockley dislocation dipole. In addition, if the triangular region is a second Frank dislocation loop overlapping the hexagonal loop, the Burgers vector of the dislocation along GE would be $\frac{1}{3}[\bar{1}\bar{1}\bar{1}]$. Computations of images of these four situations involving edge dislocations along GE were made for the range of separations 50–250 Å for both the $\bar{1}\bar{1}1$ reflection in the [516] and the 020 reflection in the [103] beam directions. A match for both experimental images simultaneously was found only for a fault step involving a $\frac{1}{6}[\bar{1}\bar{1}0]$ stair-rod dipole and intrinsic faulting on the $(\bar{1}\bar{1}1)$ plane, the dipole separation being in the range 150–180 Å. This identification was confirmed by computing the contrast for the remaining reflecting vectors at a separation of 180 Å only, for all edge situations. Figure 7 shows the computed images for this separation. Good matches for individual reflections could be obtained with other dislocation arrangements, but only the $\frac{1}{6}[\bar{1}\bar{1}0]$ step gave consistent matching at constant separation for all reflecting vectors.

Computations for the contrast along FG for all possible edge dislocation arrangements and all reflecting vectors were made at a separation of 180 Å. Consistent matching of the computed and experimental images was obtained for a faulted step involving $\frac{1}{6}[0\bar{1}\bar{1}]$ stair-rod dislocations and intrinsic faulting on $(1\bar{1}\bar{1})$.

From the matching of computed and experimental images for the edges EF, FG, and GE, it is concluded that the configuration is a stepped loop with the edges FG and GE bounded by low energy stair-rod dislocations and the side EF, a dissociated Frank dislocation.

An example of a complex loop, where it is not known whether the bend at the step is acute or obtuse or whether the dislocations bordering the step are in edge orientation, is shown in Figure 8.

The complex loop ABDCEF is on (111) with a step AB along $[\bar{1}01]$. The loop does not intersect either surface of the foil, although it approaches close to the top and bottom surfaces at B and A respectively. It was not known whether edge dislocations bordered the step on $(1\bar{1}1)$ since the image for the $\bar{2}02$ reflection was not obtained. Further, the fringe shift across the step suggested either a step height of approximately $0\cdot25\xi_{111}$ at an obtuse bend, or a step height of approximately $0\cdot75\xi_{111}$ at an acute bend. Matching the intensities of fringes across the step suggested an acute bend with the larger step height. In this case, all stair-rod dislocations of the type listed in Table 1 together with the three possible Shockley dipoles and a Frank dipole were considered in the comparisons of experimental and computed images.

Figs 8(*a*)–8(*h*).—Comparison of experimental ($\times 90\,000$) and computed images at the step AB in a complex loop in a copper–aluminium (9·4 at.%) alloy:

$\boldsymbol{FN}$ [379], $\boldsymbol{u}$ $[\bar{1}01]$, $t = 6\cdot5\xi_{111}$.

The operative reflections used, the Burgers vectors corresponding to the various computed images, and the values of $\boldsymbol{B}$ and w are indicated. In all cases the separation of the dislocations at the step along AB is $0\cdot75\xi_{111}$. Line resolution is 50 Å.

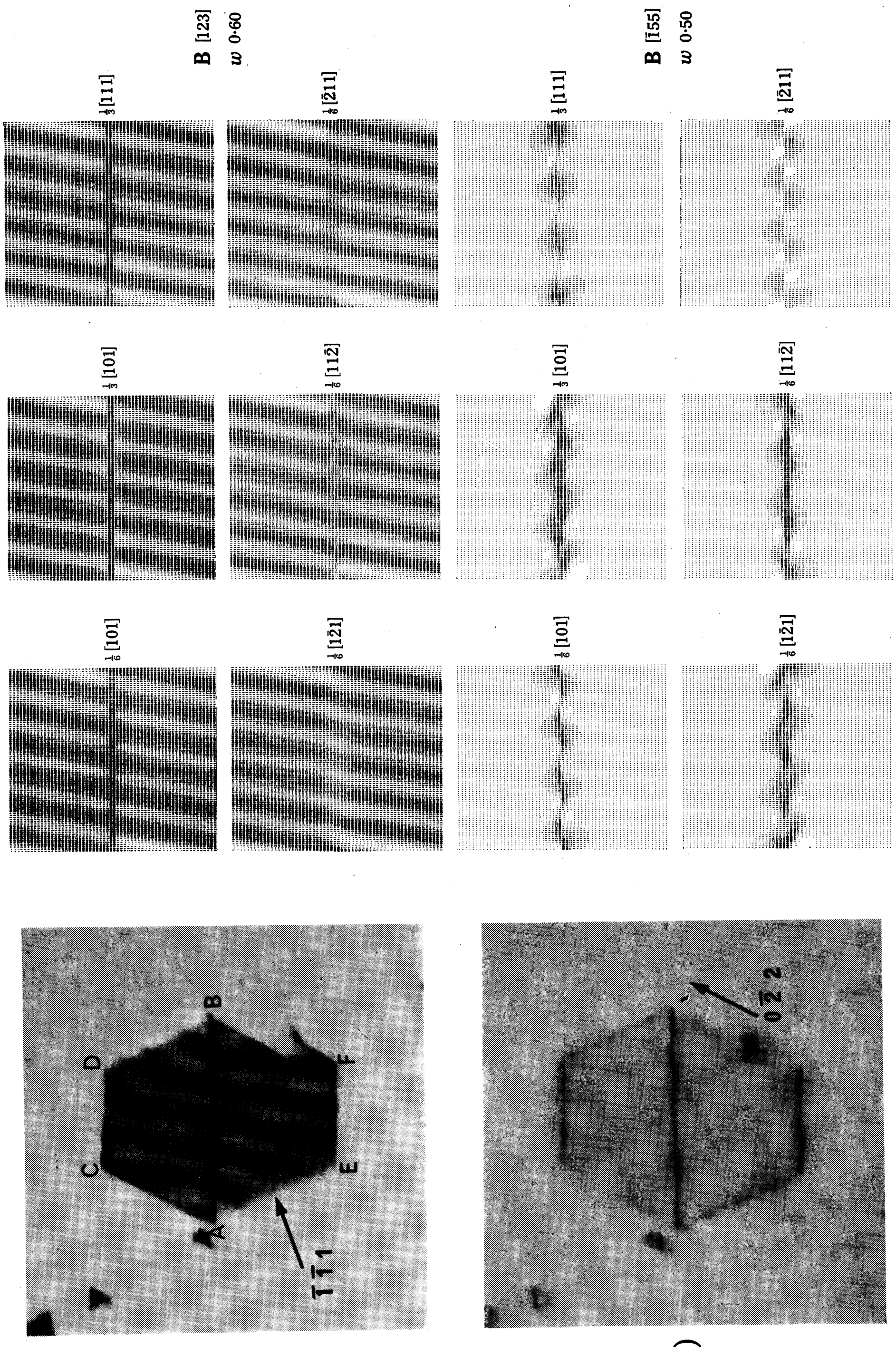

B [123]
w 0·60
$\frac{1}{3}[111]$
$\frac{1}{3}[101]$
$\frac{1}{6}[101]$
$\frac{1}{6}[\bar{2}11]$
$\frac{1}{6}[11\bar{2}]$
$\frac{1}{6}[1\bar{2}1]$
A
B
C
D
E
F
$\bar{1}\bar{1}1$
B [$\bar{1}$55]
w 0·50
$\frac{1}{3}[111]$
$\frac{1}{3}[101]$
$\frac{1}{6}[101]$
$\frac{1}{6}[\bar{2}11]$
$\frac{1}{6}[11\bar{2}]$
$\frac{1}{6}[1\bar{2}1]$
$0\bar{2}2$

8(*a*)

8(*b*)

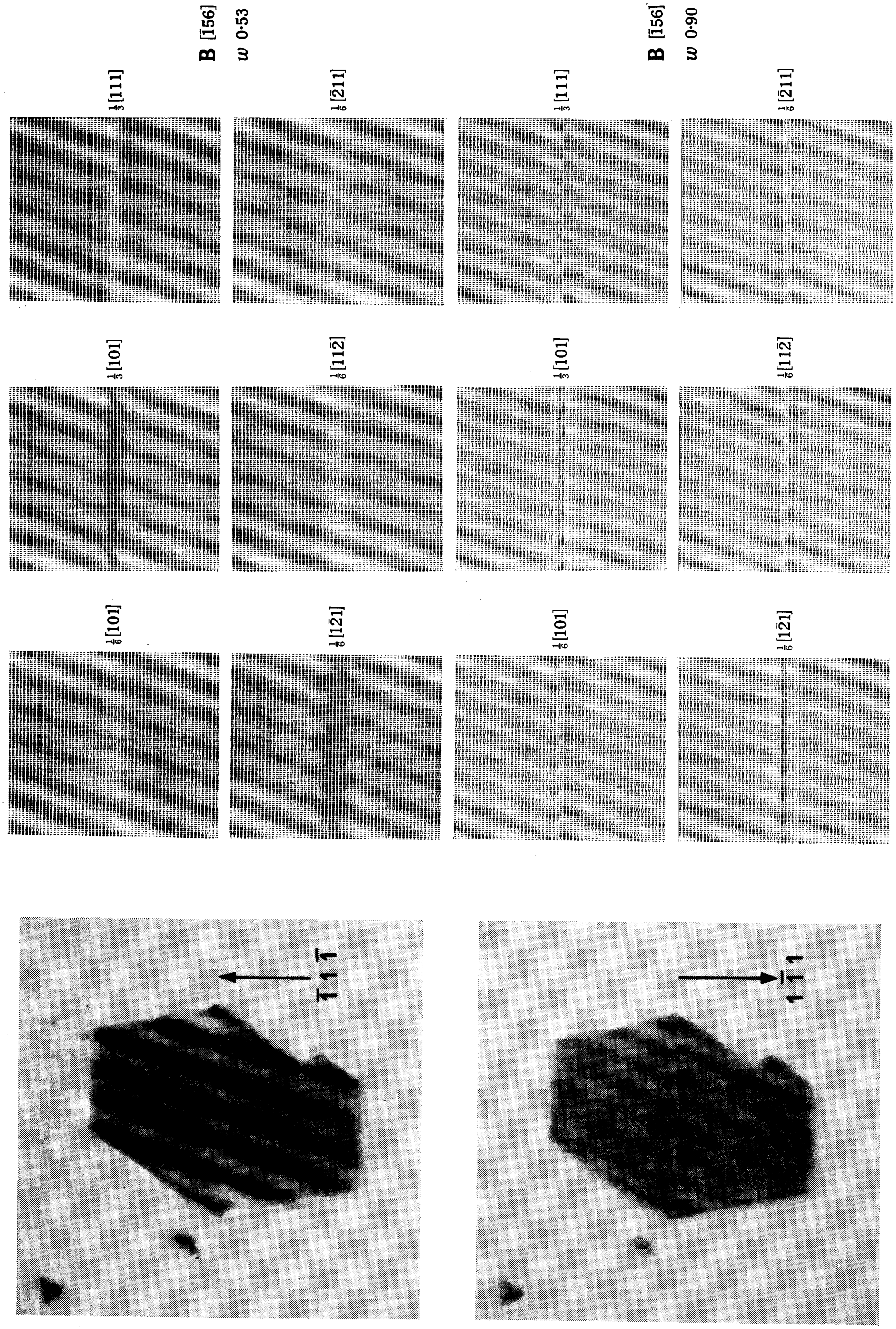

B $[\bar{1}56]$
w 0·53
$\frac{1}{3}[111]$
$\frac{1}{3}[101]$
$\frac{1}{6}[101]$
$\frac{1}{6}[\bar{2}11]$
$\frac{1}{6}[11\bar{2}]$
$\frac{1}{6}[1\bar{2}1]$
$\bar{1}\,1\,\bar{1}$
B $[\bar{1}56]$
w 0·90
$\frac{1}{3}[111]$
$\frac{1}{3}[101]$
$\frac{1}{6}[101]$
$\frac{1}{6}[\bar{2}11]$
$\frac{1}{6}[11\bar{2}]$
$\frac{1}{6}[1\bar{2}1]$
$1\,\bar{1}\,1$

8(*c*)

8(*d*)

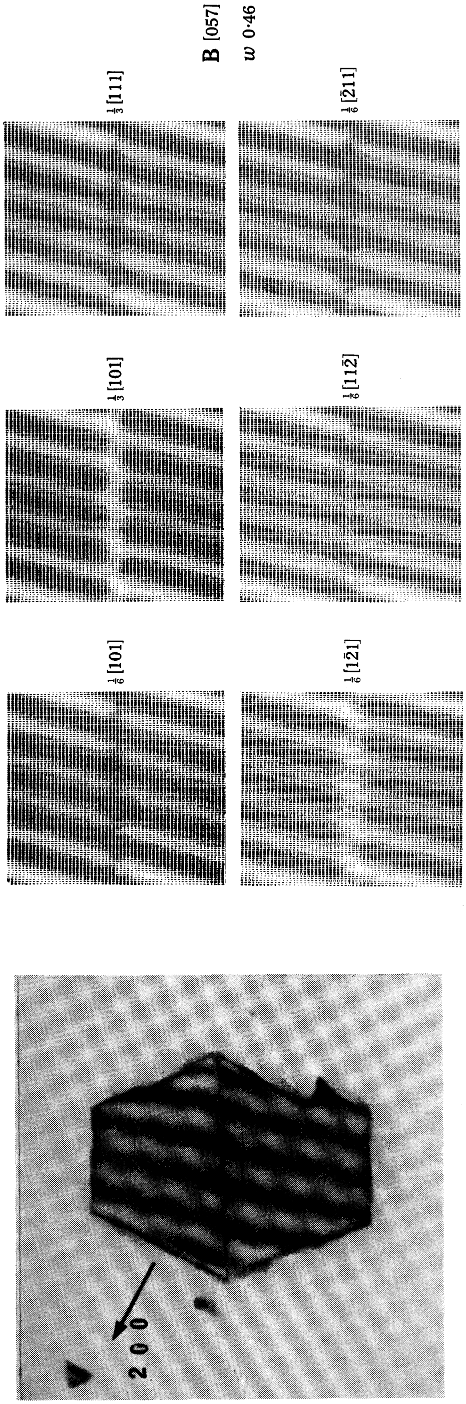
B [057]
w 0·46
1/3[111]
1/3[101]
1/6[101]
1/6[$\bar{2}$11]
1/6[11$\bar{2}$]
1/6[1$\bar{2}$1]
2 0 0

8(e)

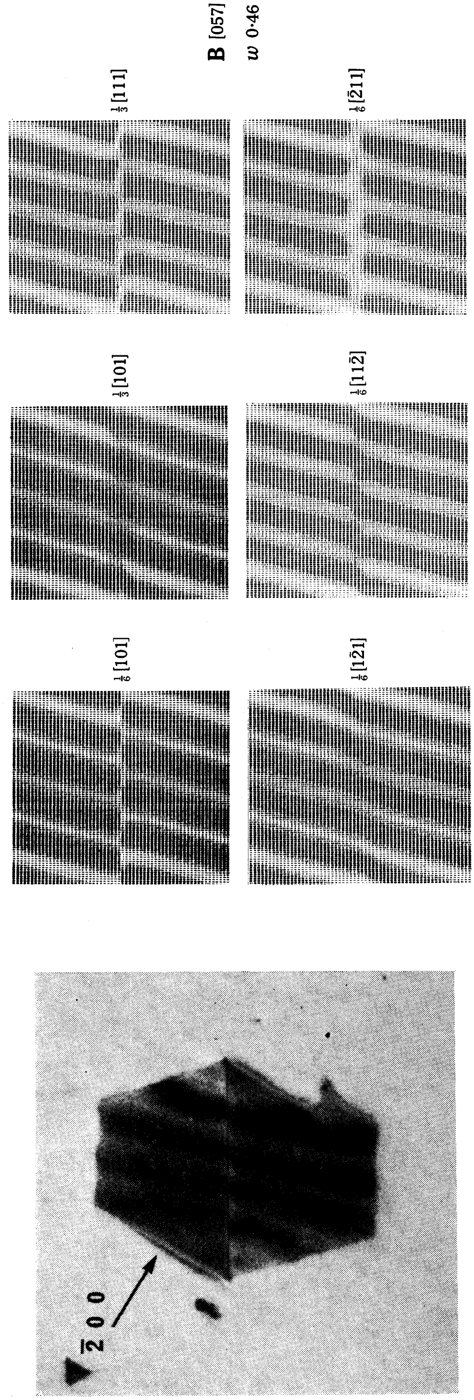
B [057]
w 0·46
1/3[111]
1/3[101]
1/6[101]
1/6[$\bar{2}$11]
1/6[11$\bar{2}$]
1/6[1$\bar{2}$1]
$\bar{2}$ 0 0

8(f)

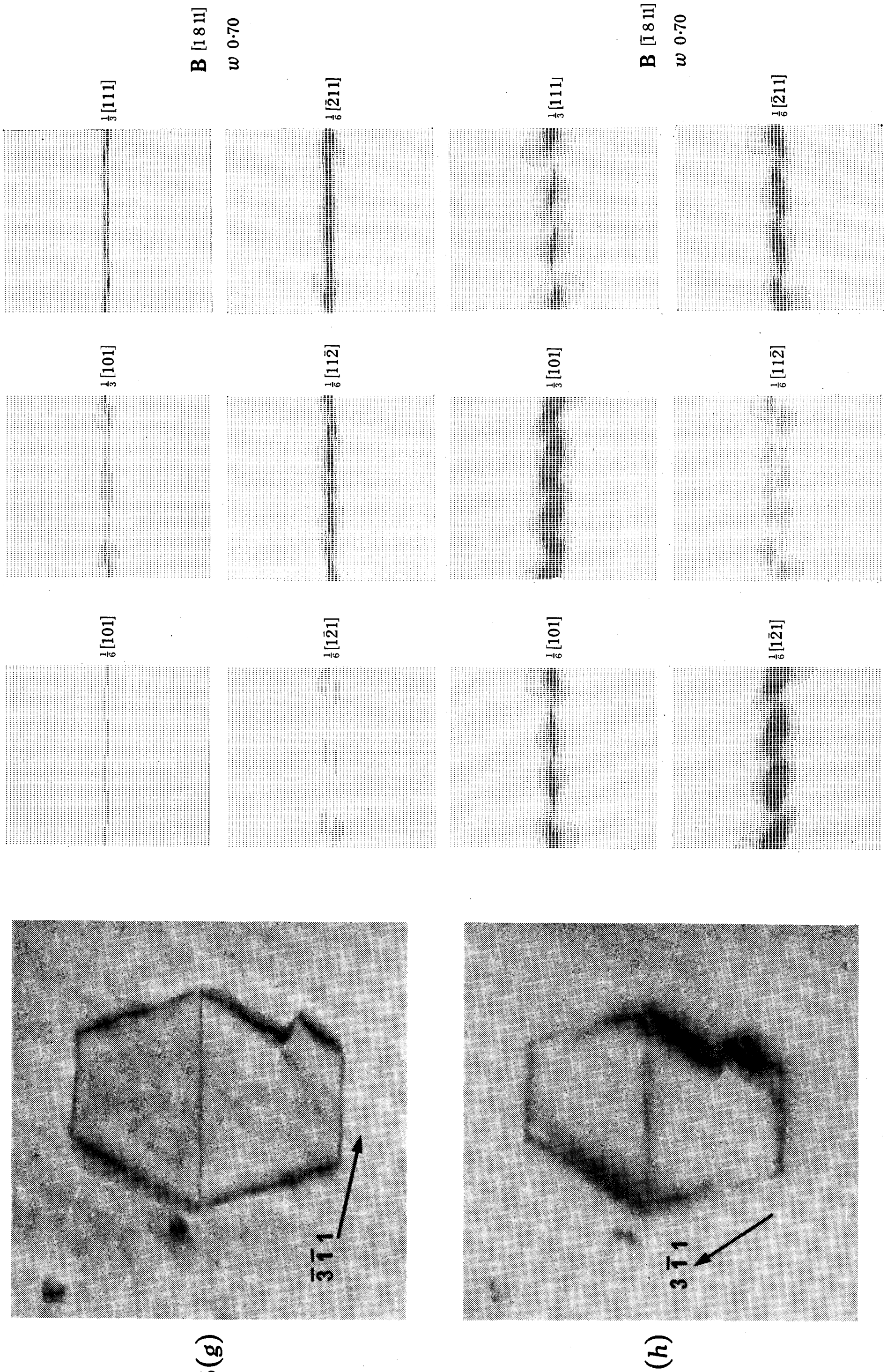
B [1 8 11]
w 0·70
$\frac{1}{3}[111]$
$\frac{1}{3}[101]$
$\frac{1}{6}[101]$
$\frac{1}{6}[\bar{2}11]$
$\frac{1}{6}[11\bar{2}]$
$\frac{1}{6}[1\bar{2}1]$
B [$\bar{1}$ 8 11]
w 0·70
$\frac{1}{3}[111]$
$\frac{1}{3}[101]$
$\frac{1}{6}[101]$
$\frac{1}{6}[\bar{2}11]$
$\frac{1}{6}[11\bar{2}]$
$\frac{1}{6}[1\bar{2}1]$
$\bar{3}\,\bar{1}\,1$
$3\,\bar{1}\,1$

8(g)

8(h)

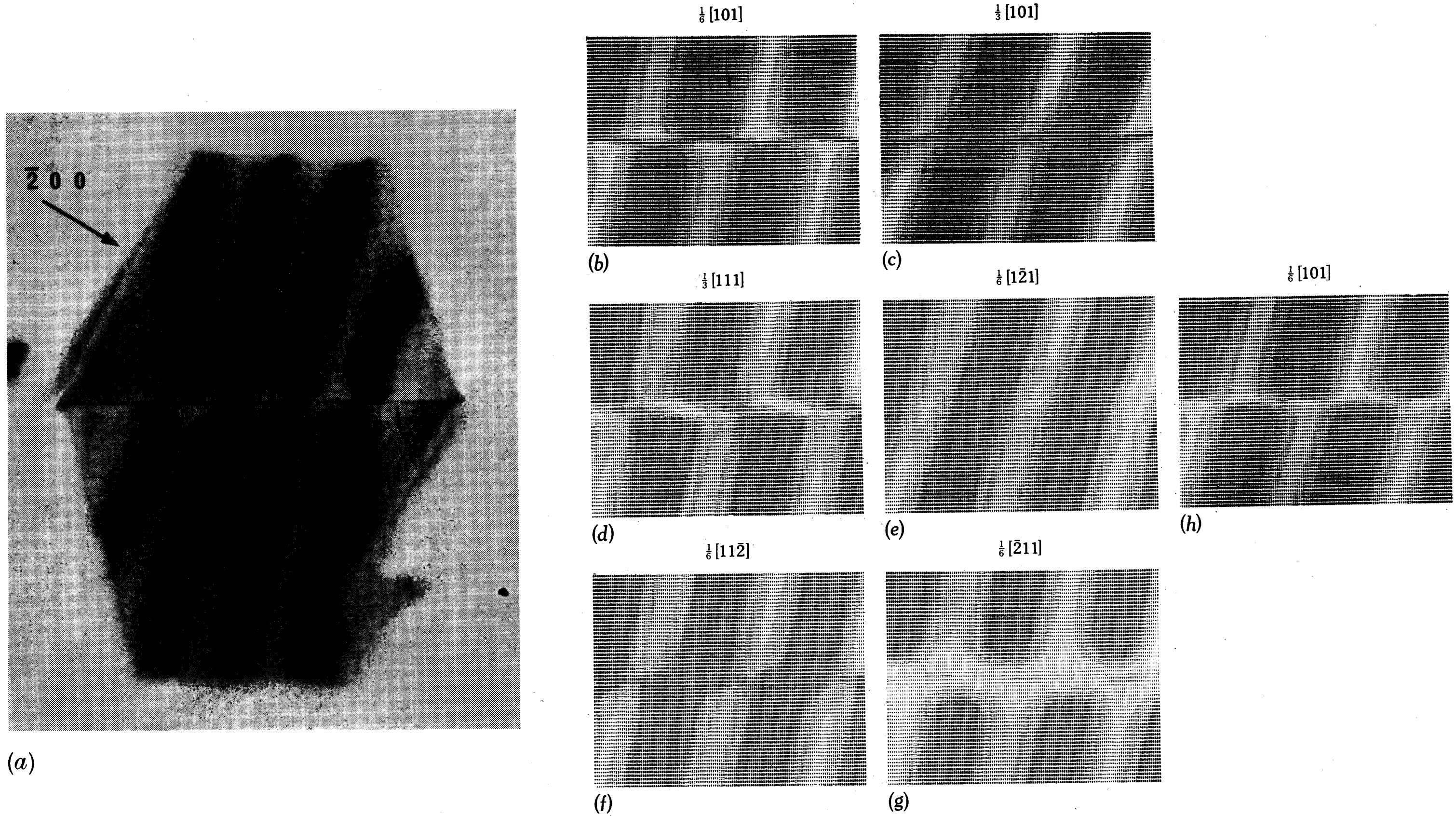

Fig. 9.—Comparison of high magnification experimental ($\times 200\,000$) and computed images corresponding to Figure 8(f) and the influence of beam direction on image detail ($\boldsymbol{B}$ is [057] in (b)–(g) and [011] in (h)):

$$\boldsymbol{FN}\ [379] \qquad \boldsymbol{u}\ [\bar{1}01], \qquad t = 6\cdot5\xi_{111}, \qquad w = 0\cdot46.$$

The Burgers vectors corresponding to the various computed images are indicated. In all cases the separation of the dislocations at the step along AB is $0\cdot75\xi_{111}$. The images are computed between $1\cdot5$ and $3\cdot5\xi_{200}$ from the top surface and the portion of the micrograph (a) corresponding to the computed images is indicated. Line resolution is 20 Å.

Matching between experimental and computed images for the $\bar{1}1\bar{1}$ and $1\bar{1}1$ reflections, and all possible values for the Burgers vectors of dislocations bordering the step, was investigated for an obtuse bend with a step height of $0\cdot25\xi_{111}$. In no case was there good agreement between experimental and computed images, thus supporting the tentative conclusion from the fringe matching that the step is acute.

The computed images for the possible Burgers vectors of dislocations bordering an acute bend with a step height of $0\cdot75\xi_{111}$ are compared with the experimental images in Figures 8(*a*)–8(*h*). It can be seen that agreement between the computed and experimental images for all the reflections is only obtained with the $\frac{1}{6}[101]$ Burgers vector.

A feature of the $\bar{2}00$ image in Figure 8(*f*) is the fine dark line, approximately 30 Å wide, along AB. This detail appears in the computed image only if the true beam direction, [057], for which the loop plane (111) and the step plane $(1\bar{1}1)$ overlap, is used. This can be seen in Figure 9, where the experimental image and high-magnification computed images for the $\frac{1}{6}[101]$ Burgers vector and beam directions [057] and [011] are given (compare Fig. 9(*b*) with 9(*h*)). Further, it can be seen from Figure 9 that, although a fine dark line appears in the computed images for the $\frac{1}{6}[101]$ and $\frac{1}{3}[101]$ Burgers vectors, the fine detail of the experimental image is matched only by the computed image for the $\frac{1}{6}[101]$ Burgers vector. It is concluded that the step in this loop is bounded by $\frac{1}{6}[101]$ and $\frac{1}{6}[\bar{1}0\bar{1}]$ stair-rod dislocations at a separation of approximately 180 Å.

An example of a loop where the step is known to be acute is given in Figures 10(*a*)–10(*g*), and in this case only the computed images considered to give the best match to the experimental images are presented. The loop ABCDEF is on (111) with the step FD along $[\bar{1}10]$ so that the plane of the step is $(11\bar{1})$. The loop intersects the top surface of the foil along CDE. From the fringe shift at the surface, the fault to the left of F $\rightarrow$ D lies below the fault to the right, indicating an acute bend for a step on $(11\bar{1})$ with a step height of approximately $0\cdot5\xi_{111}$.

The possible Burgers vectors for the dislocations bordering the step in this case are the stair-rods $\frac{1}{6}[110]$ or $\frac{1}{3}[110]$ for a faulted step and the Shockleys $\frac{1}{6}[2\bar{1}\bar{1}]$, $\frac{1}{6}[\bar{1}2\bar{1}]$, $\frac{1}{6}[\bar{1}\bar{1}2]$, or the Frank $\frac{1}{3}[111]$ for an unfaulted step. Images have been computed for all these possible Burgers vectors and the best match between the experimental and theoretical images is obtained for a step bounded by $\frac{1}{6}[110]$ and $\frac{1}{6}[\bar{1}\bar{1}0]$ stair-rod dislocations at a separation of 120 Å.

The fine detail in the experimental images is reproduced in the computed images for comparable resolution in both (Fig. 10). Thus for the $\bar{1}\bar{1}1$ reflection, the rounded protrusion at the end of the dark fringe at the surface intersection D is reproduced

---

Fig. 10 (*opposite*).—Comparison of experimental and computed images at the step FD in a complex loop in a copper–aluminium (9·4 at.%) alloy. In (*a*)–(*c*) the comparisons are made with the experimental images ×98 000 and in (*d*)–(*g*) with the 200 image ×320 000:

$$\boldsymbol{FN}\ [157], \qquad \boldsymbol{u}\ [\bar{1}10], \qquad t = 6\xi_{111}.$$

The portion of the micrograph (*d*) corresponding to the images (*e*)–(*g*) and the values of ***B***, ***g***, and *w* are indicated. All computed images are for $\frac{1}{6}[110]$ stair-rod dislocations bordering the step at a separation of $0\cdot5\xi_{111}$. Line resolution is 30 Å in (*a*)–(*c*) and 11 Å in (*e*)–(*g*).

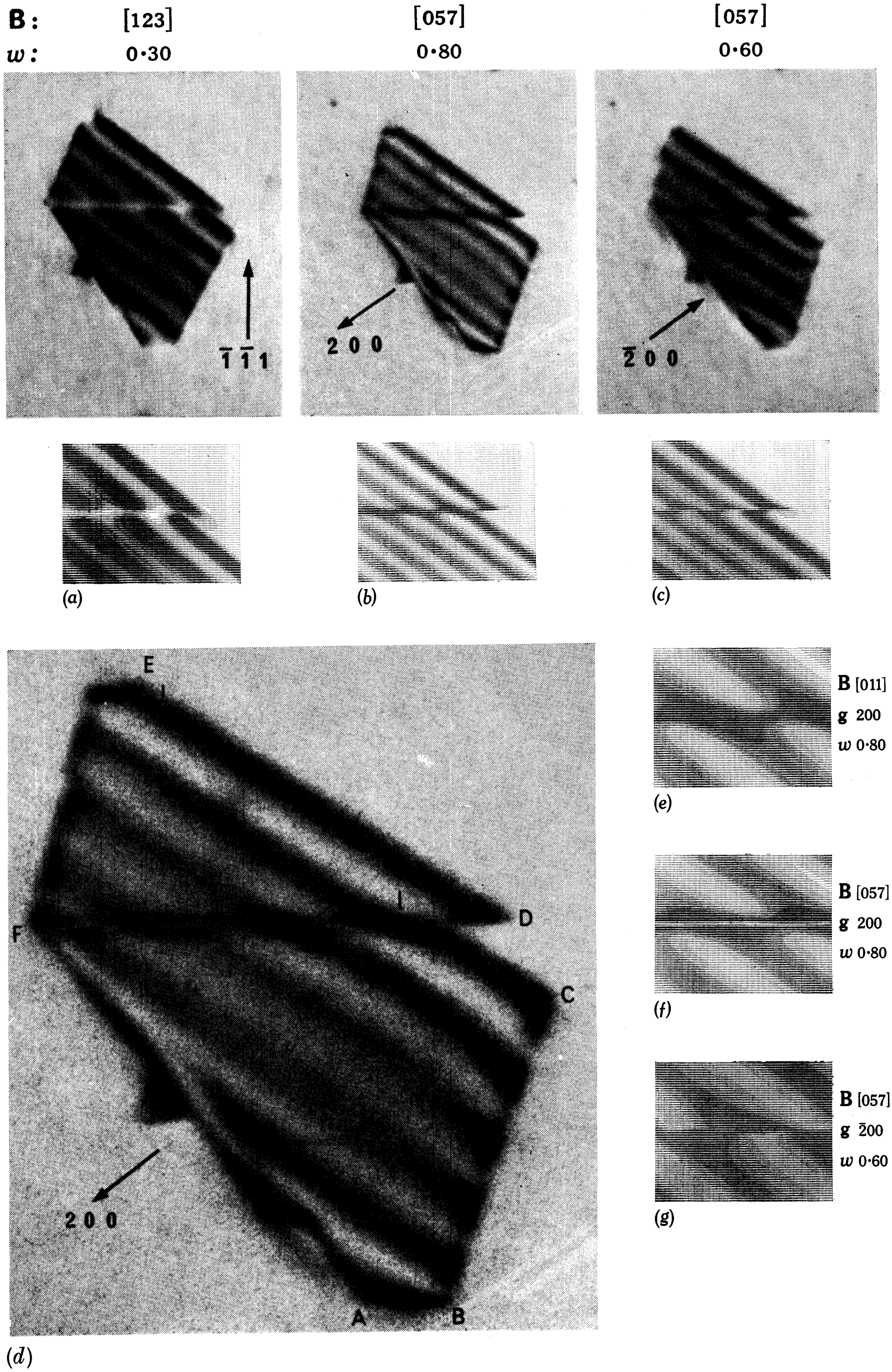
B: [123] [057] [057]
w: 0·30 0·80 0·60
$\bar{1}\bar{1}1$
2 0 0
$\bar{2}$ 0 0
(a)
(b)
(c)
E
D
F
C
2 0 0
A
B
(d)
B [011]
g 200
w 0·80
(e)
B [057]
g 200
w 0·80
(f)
B [057]
g $\bar{2}$00
w 0·60
(g)

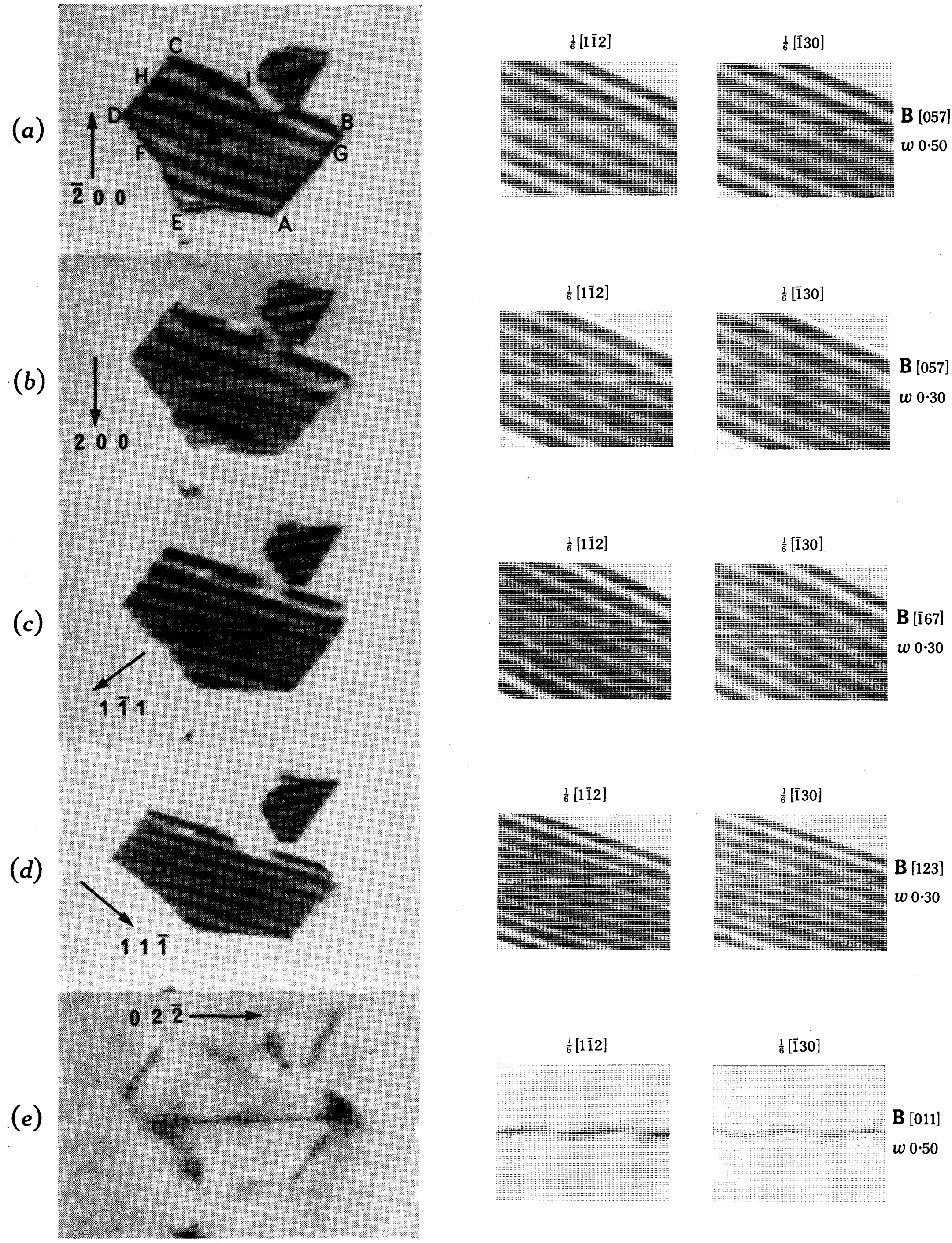
(a)
C
H
I
D
B
F
G
2̄ 0 0
E
A
⅙ [1 1̄ 2]
⅙ [1̄ 3 0]
B [057]
w 0·50
(b)
2 0 0
⅙ [1 1̄ 2]
⅙ [1̄ 3 0]
B [057]
w 0·30
(c)
1 1̄ 1
⅙ [1 1̄ 2]
⅙ [1̄ 3 0]
B [1̄67]
w 0·30
(d)
1 1 1̄
⅙ [1 1̄ 2]
⅙ [1̄ 3 0]
B [123]
w 0·30
(e)
0 2 2̄
⅙ [1 1̄ 2]
⅙ [1̄ 3 0]
B [011]
w 0·50

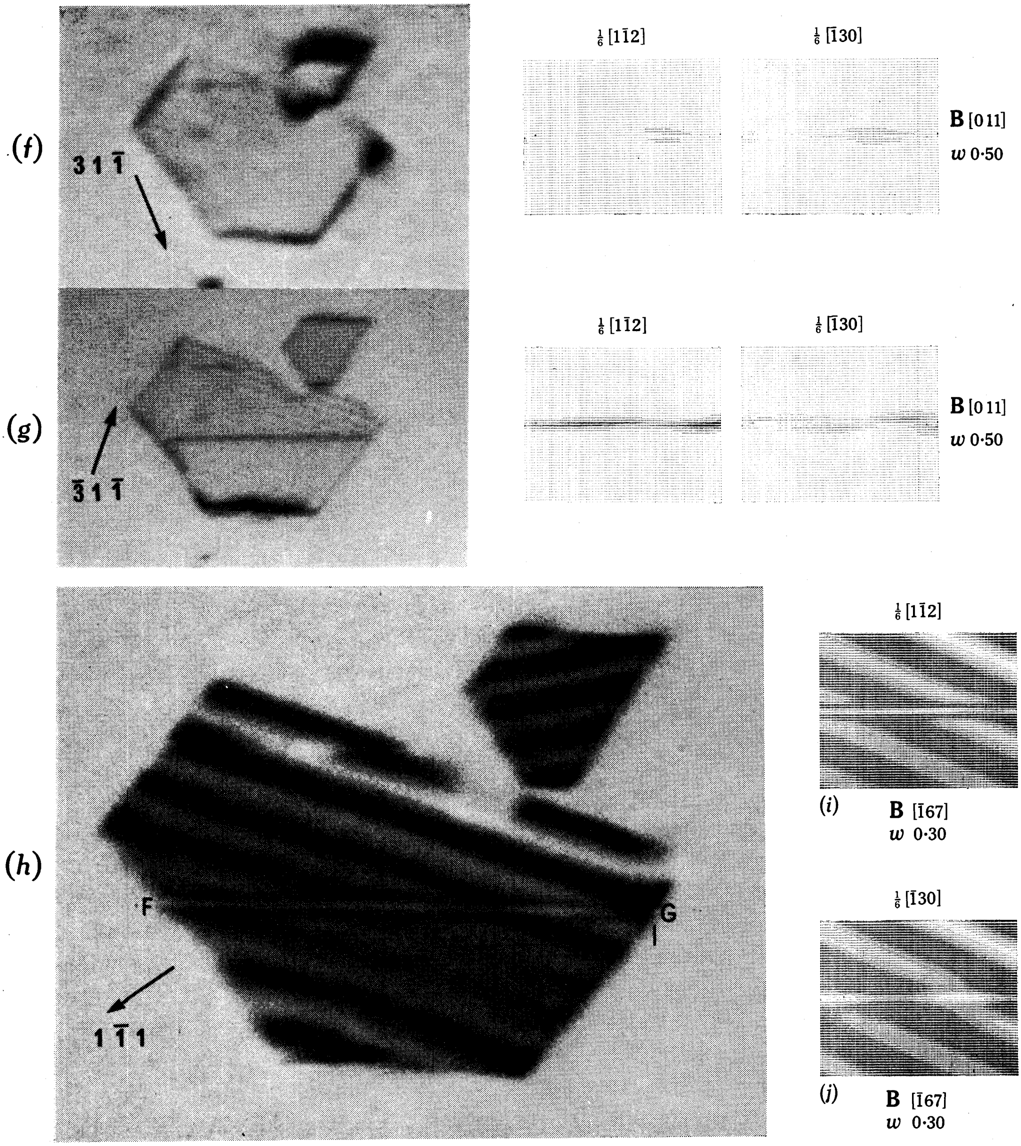

Figs 11(*a*)–11(*j*).—Comparison of experimental and computed images at the step FG in a complex loop in a copper–aluminium (9·4 at.%) alloy. In (*a*)–(*g*) the comparisons are made with the experimental images $\times 90\,000$ and in (*h*)–(*j*) with the $1\bar{1}1$ image $\times 200\,000$:

$$\boldsymbol{FN}\ [123], \qquad \boldsymbol{u}\ [0\bar{1}1], \qquad t = 7\xi_{111}.$$

The operative reflections, the Burgers vectors corresponding to the computed images, and the values of ***B*** and w are indicated. In all cases the separation of the dislocations at the step along FG is $0\cdot25\xi_{111}$. The portion of the experimental image (*h*) corresponding to the computed images (*i*) and (*j*) is indicated. Line resolution is 55 Å in (*a*)–(*g*) and 25 Å in (*i*) and (*j*).

in the computed image, as is the region clearly above background intensity in the first light fringe at the step (Fig. 10(a)). Further, the general shape of the light band at the step is reproduced in the computed image (Fig. 10(a)). The curvature of the fringes in the 200 image, suggesting a point of inflexion at the step, is reproduced in the computed image (Fig. 10(b)), but at this magnification the fine detail of the contrast along the step is not resolved. The contrast along the step in Figure 10(b) consists of a fine light band, approximately 50 Å wide, bordered by dark lines that are narrow and faint where they pass through the light fringes and broader and darker where they pass through the dark fringes at the step. Further, in the light fringes the lower of the two lines appears very weak. This light band and its associated detail are not present in the $\bar{2}00$ image. The experimental 200 image and computed images at higher magnification for 200 and $\bar{2}00$ reflections are given in Figures 10(d)–10(g). It can be seen that the computed image at this magnification reproduces the fine detail in the experimental image for the 200 reflection and confirms the absence of any resolution for the $\bar{2}00$ reflection.

It should be noted that for the loops shown in Figures 9 and 10, the matching of the fine image detail at the fault bend is obtained only when the precise beam direction rather than the approximate beam direction is used in the computations. This applies both when the faults viewed in the beam direction are overlapping (Figs 9(b) and 9(h)) and when they are non-overlapping (Figs 10(e) and 10(f)).

The complex loop in Figures 11(a)–11(j) is an example of non-edge dislocations bordering the step, i.e. strong contrast is observed with a 220 diffracting vector parallel to the step. The loop ABCDE (Fig. 11(a)) is unusually complex in that two bands of contrast FG and HI cross the stacking fault fringes along $[0\bar{1}1]$. The loop lies on $(\bar{1}11)$ and intersects the bottom of the foil along BC. From the direction of the fringe shift at the bottom surface, the fault to the right of H $\rightarrow$ I must lie below the fault to the left and, assuming that the contrast arises from a step in the fault with the step on (111), the observed fringe shift corresponds to an obtuse bend. Matching fringes across FG gives a fringe shift in the same sense as for HI, indicating that the fault to the right of F $\rightarrow$ G lies below the fault to the left, and again suggesting an obtuse bend in the stacking fault. Thus the defects along HI and FG are taken to be associated with obtuse bends in an intrinsic fault.

The absence of contrast along HI for the $02\bar{2}$ reflection shows that this step is bounded by edge dislocations. However, for the 200 and 111 reflections, details of the contrast associated with HI can only be seen for approximately one extinction distance below the surface and this was not sufficient for a detailed comparison of experimental and computed images. Thus no decision could be reached between the various possibilities for the Burgers vectors of the dislocations at this step.

The contrast along FG is strong for the $02\bar{2}$ reflection (Fig. 11(e)), indicating that non-edge dislocations are associated with this step. The $1\bar{1}1$ reflection gives the most striking image in Figure 11. For this reflection, the image along FG consists of a light band bordered on both sides by dark lines. The $11\bar{1}$ image is mainly light with some contrast at the step in the region of the dark fringes. The 200 and $\bar{2}00$ images are mainly light with the $\bar{2}00$ image showing some fringe contrast at the step. The $\bar{3}1\bar{1}$ image shows contrast along FG, but contrast is absent on $31\bar{1}$.

The dislocations along FG are not in edge orientation, so that several possibilities such as Frank partials, edge Shockley partials, and low energy stair-rods associated with extrinsic faulting in an obtuse step are excluded. There are six remaining possible values of $\boldsymbol{b}$ for dislocation dipoles along FG. Four of these ($\frac{1}{6}[1\bar{3}0]$, $\frac{1}{6}[103]$, $\frac{1}{6}[130]$, $\frac{1}{6}[10\bar{3}]$) involve high energy stair-rod dislocations and two ($\frac{1}{6}[12\bar{1}]$ and $\frac{1}{6}[1\bar{1}2]$) Shockley partial dislocations bordering an unfaulted step. The fringe shift for the 111 reflections in Figures 11(c) and 11(d) is small and suggests a step height of approximately $0\cdot25\xi_{111}$. In fact, the best fits between experimental and theoretical images for all the possible Burgers vectors were obtained at this step height. Images have been computed for all the above values of $\boldsymbol{b}$ and the two possibilities which give the best match to the experimental images are $\frac{1}{6}[\bar{1}30]$ and $\frac{1}{6}[1\bar{1}2]$. The computed images for these values of $\boldsymbol{b}$ are compared with the experimental images in Figures 11(a)–11(j). For the 200 reflection, the contrast along FG appears too dark for $\boldsymbol{b} = \frac{1}{6}[\bar{1}30]$, but there is little to choose between the two values of $\boldsymbol{b}$ for the $\bar{2}00$ images. For $\boldsymbol{b} = \frac{1}{6}[\bar{1}30]$ the $11\bar{1}$ reflection gives too much dark contrast in the light fringes crossing FG and the $\bar{3}1\bar{1}$ and $02\bar{2}$ images appear to be too weak. These results when combined with the **111** image enable a decision to be made between the two Burgers vectors. Experimental and theoretical images at higher magnification are shown for the $1\bar{1}1$ reflection in Figures 11(h)–11(j). At the low magnification (Fig. 11(c)) the high energy stair-rod dipole appears a better fit, but at the higher magnification, where the resolution in the computed images is comparable with the experimental resolution, it can be seen that the image of the Shockley dipole (Fig. 11(i)) matches the fine detail in the experimental image in that a light band bordered on both sides by a dark line traverses the fringes along FG. For the stair-rod dipole the dark lines do not appear (Fig. 11(j)). It is concluded from this comparison of experimental and computed images that the step along FG is obtuse, unfaulted, and bounded by $\frac{1}{6}[1\bar{1}2]$ and $\frac{1}{6}[\bar{1}1\bar{2}]$ Shockley dislocations at a separation of approximately 60 Å.

The small loop in Figure 2 also contains a step bounded by non-edge dislocations. This loop lies on (111) with a step along $[0\bar{1}1]$. Comparison of experimental and computed images for the $\bar{1}\bar{1}1$, $\bar{1}1\bar{1}$, $1\bar{1}1$, 200, $\bar{2}00$, $3\bar{1}1$, $\bar{3}\bar{1}1$, and $0\bar{2}2$ reflections for all possible values of the Burgers vector of dislocations bounding the step indicates that in this case also the step is obtuse, unfaulted, and bounded by $\frac{1}{6}[1\bar{2}1]$ and $\frac{1}{6}[\bar{1}2\bar{1}]$ Shockley dislocations at a separation of approximately 70 Å.

Because of the large amount of computation involved in positively identifying the Burgers vectors of dislocations at steps in complex loops, only a small number of cases have been treated fully. Complete computations of all possibilities resulting in positive identification of $\frac{1}{6}\langle110\rangle$ Burgers vectors have been done for seven cases. Further, complete computations have been done for the two cases found to involve non-edge dislocations giving $\frac{1}{6}\langle112\rangle$ Burgers vectors in both. Several other cases involving edge dislocations have been partially computed, and these also suggest $\frac{1}{6}\langle110\rangle$ Burgers vectors. These numbers grossly overestimate the ratio of $\frac{1}{6}\langle112\rangle$ to $\frac{1}{6}\langle110\rangle$ Burgers vectors as a deliberate effort was made to find non-edge dislocations at steps.

VI. Additional Computations

It is to be expected that only steps above a certain minimum height can be detected from diffraction contrast. Computations for Shockley and stair-rod dipoles show that steps approximately 20 Å high would be difficult to detect experimentally and contrast effects in computed images become negligible at step heights less than 10 Å. Thus the observed density of complex loops must be an underestimate.

The formation of stepped loops, either by combination or by fault climb, resulting in extrinsic faults in the steps, is unlikely. However, it is possible that an extrinsic fault in a step could result from the nucleation of a vacancy loop at a completed step, so as to form overlapping intrinsic faults in the step. In this case, the two dislocations along each edge of the doubly faulted step will have $\frac{1}{6}\langle 110\rangle$ and $\frac{1}{3}\langle 111\rangle$ Burgers vectors. Since these dislocations are separated only by one plane, they may be regarded for purposes of image computation as a single dislocation of the form $\frac{1}{6}\langle 332\rangle$. Computations of the contrast for such combinations of intrinsic faults have been made in a few instances, and these images did not match the experimental images.

VII. Discussion

Two points of interest relating to diffraction contrast arise from the comparison of experimental and computed images. Firstly, it has been observed that small variations in the electron beam direction may produce marked changes in the nature of the image and this is to be expected for the complex configuration of dislocations and stacking faults considered here, in contrast to the behaviour of a single dislocation (Head, Loretto, and Humble 1967). Secondly, the computations using the Head–Humble technique are based on the Howie–Whelan two-beam column approximation (Howie and Whelan 1961), and it is of interest that this approximation is capable of reproducing image detail involving resolution of approximately 30 Å.

In analysing the Burgers vectors associated with the steps, image computations were only carried out for two dislocations and three stacking faults. Thus the possibility of two Frank loops dissociated on neighbouring planes, so as to form an incomplete step, was not considered as this involves four dislocations and four stacking faults. Whilst such a configuration may give contrast similar to that observed for complete steps, it would be surprising if it matched all fine detail of experimental images.

The presence of stepped loops in silver and two copper–aluminium alloys and their absence in aluminium, indicates that low stacking fault energy is associated with the formation of this type of Frank loop.

We will consider two ways in which steps may form in Frank dislocation loops. Both of these involve the dissociation of the Frank dislocation loops which has been shown to occur in these materials (Clarebrough and Morton 1969*b*).

The simplest method of obtaining a step in an intrinsic Frank loop is for two loops on neighbouring planes to unite by dissociation of parallel edges on a common intersecting $\{111\}$ plane. A Frank dislocation will only lower its energy by dissociation if dissociation involves a low energy stair-rod dislocation. Thus intrinsically faulted steps that form in this way will always be acute and bounded by $\frac{1}{6}\langle 110\rangle$ dislocations along the step edges and $\frac{1}{6}\langle 112\rangle$ dislocations along the step risers. This mechanism would not be expected to operate in materials of high stacking fault energy such as aluminium where the dissociation would be very small, but could operate for the low stacking fault energy materials considered here.

It will be shown that a stepped loop could also result from climb of the stacking fault by addition of vacancies (Escaig 1963; Schapink and de Jong 1964). This mechanism will be favoured in low stacking fault energy materials because dissociation of the Frank dislocation hinders the addition of vacancies to the edge of a growing loop. The lowest energy configuration for the nucleus involved in climb is a triangular region with edges along $\langle 110\rangle$ directions (Escaig 1963). After the first climb step the triangular region is bounded by $\frac{1}{3}$ vacancy jog lines (Thompson 1955) which may be regarded as dipoles of Shockley partial dislocations. Nucleation of such a climbed region is expected to occur at the edge of a loop (Escaig 1963), in which case one edge of the climbed region is the Frank dislocation. The climbed nucleus may propagate across the loop by motion of the jog lines, the addition of one vacancy adding a complete row of atoms to the climbed region. If the climbed nucleus were hexagonal, alternate sides would be bounded by $\frac{1}{3}$ and $\frac{2}{3}$ vacancy jog lines.

The formation of large steps in complex loops is compatible with fault climb involving the nucleation and propagation of jog lines. Thus steps must occur if jog lines produce climb up and climb down in different portions of the loop. Union of such climbed regions must produce a step and continued climb will increase the step height, with climb at all stages involving the movement of jog lines.

Climb of the stacking fault surrounded by a dissociated Frank dislocation will be considered in some detail and it will be shown that constriction is not necessary for fault climb. For a dissociated loop, the favoured sense for the nucleation of climb at a particular edge is related to the sense of the dissociation. For example, the favoured sense of climb at an edge dissociated below the plane of the loop will be above the plane. The climbed regions will be taken as having nucleated and grown by the addition of vacancies to give climb above and climb below the plane of the loop as illustrated schematically in Figure 12(a). The addition of further vacancies will unite the climbed regions with one another, and with the edges of the dissociated Frank dislocation loop, and these processes will be illustrated by reactions involving Shockley dipoles. The loop is on (111) with Burgers vector $\mathbf{A}\boldsymbol{\alpha}$* and the jog lines bordering the climbed regions are denoted by the appropriate Shockley dipoles. For simplicity in illustrating the dislocation reactions involved, the climbed regions are shown in Figure 12(a) as having nucleated away from the edges of the loop.

Figure 12(b) illustrates the union of climbed regions 2 and 6 with the dissociated Frank dislocation. Figure 12(c) illustrates the union of regions 2 and 6 with one another in the region of B. Union of region 2 (climb up) with the dissociated Frank dislocation involves the reactions

$$\mathbf{C}\boldsymbol{\alpha}+\boldsymbol{\alpha\beta} = \mathbf{C}\boldsymbol{\beta}, \qquad \mathbf{BC}+\mathbf{C}\boldsymbol{\beta} = \mathbf{B}\boldsymbol{\beta}, \qquad \boldsymbol{\alpha}\mathbf{C}+\mathbf{C}\boldsymbol{\beta} = \boldsymbol{\alpha\beta},$$

and union of region 6 involves similar reactions. The formation of a nucleus of climbed fault at the edge of a dissociated Frank dislocation involves reactions of this type. When regions 2 and 6 meet (Fig. 12(c)), $\mathbf{B}\boldsymbol{\alpha}$ and $\boldsymbol{\alpha}\mathbf{B}$ annihilate and the reactions

$$\mathbf{B}\boldsymbol{\beta}+\boldsymbol{\beta}\mathbf{A} = \mathbf{BA} \qquad \text{and} \qquad \mathbf{A}\boldsymbol{\gamma}+\boldsymbol{\gamma}\mathbf{B} = \mathbf{AB}$$

occur to give an unfaulted step with the dislocation $\mathbf{AB}$ along the step riser XY

* Thompson's (1953) notation is used to denote the Burgers vectors of dislocations.

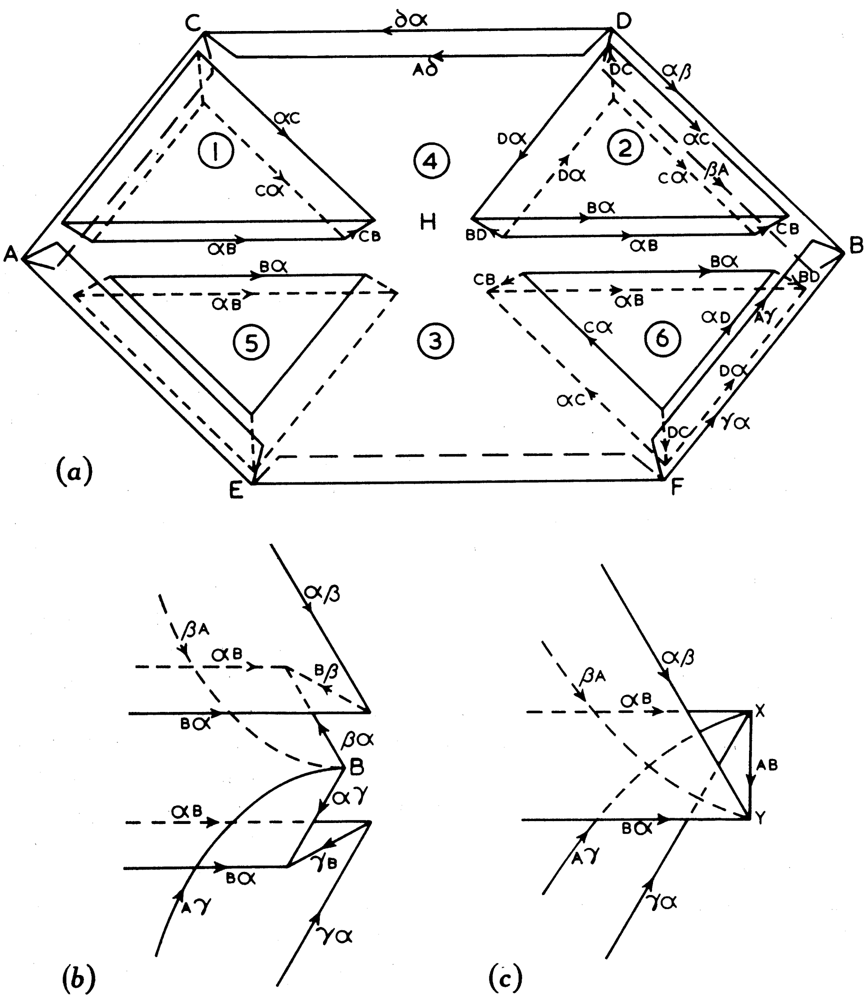

Fig. 12.—Schematic illustrations of: (*a*) a dissociated Frank dislocation loop with alternate edges dissociated above and below the plane of the loop; in regions 1 and 2 fault climb is above the plane of the loop and in regions 5 and 6 below the plane of the loop; (*b*) portion of the loop in (*a*) after regions 2 and 6 have combined with the dissociated Frank dislocation; and (*c*) portion of the loop in (*a*) after regions 2 and 6 have combined with one another.

and with the dissociated Frank dislocation now constricting at the new nodes X and Y. The dislocation **AB**, on $(11\bar{1})$, probably decreases its line length by glide to lie along a $\langle 112 \rangle$ direction.

Figure 13 illustrates the union of climbed regions 1 and 2 at H (Fig. 12(*a*)), at the stage when these climbed regions first meet (Fig. 13(*a*)) and after the union has progressed to some extent (Fig. 13(*b*)). The reactions involved are

$$\mathbf{CB} + \mathbf{BD} = \mathbf{CD} \qquad \text{and} \qquad \mathbf{D\alpha} + \boldsymbol{\alpha}\mathbf{C} = \mathbf{DC}\,.$$

The union of region 2 with the dissociated Frank dislocation in the vicinity of D (Fig. 12(*a*)) may be considered in the following way. The shear involved in the

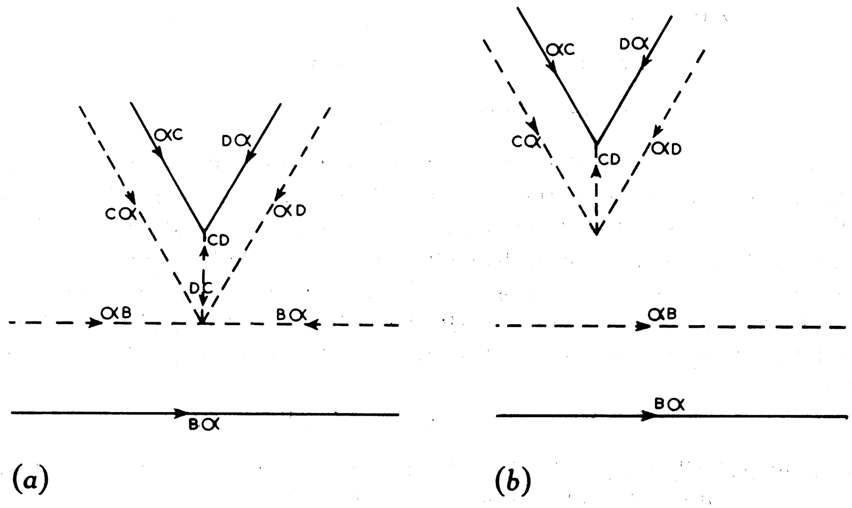

Fig. 13.—Schematic illustrations of the union of climbed regions 1 and 2 at H (Fig. 12(a)): (a) immediately after union, (b) after union has progressed to some extent.

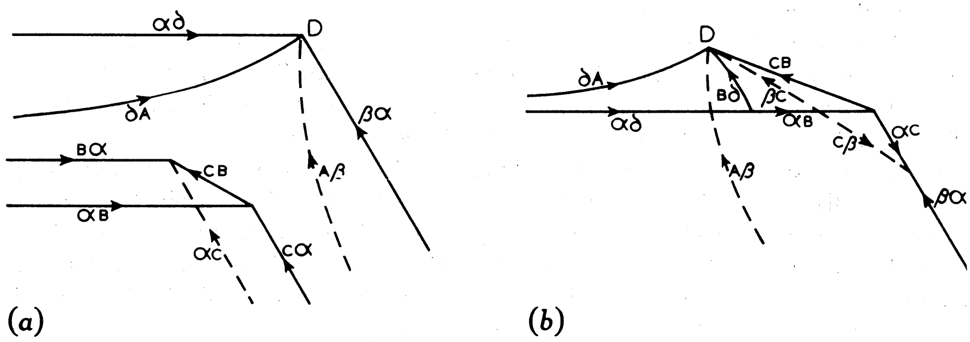

Fig. 14.—Schematic illustrations of the union of region 2 with the dissociated Frank dislocation at D (Fig. 12(a)): (a) $\frac{2}{3}$ vacancy jog line formed, (b) reaction between $\frac{2}{3}$ vacancy jog line and dissociated Frank dislocation.

union of 1 and 2 at H introduces a length of $\frac{2}{3}$ vacancy jog line on region 2 at the corner near D, as illustrated in Figure 14(a). The reactions between the $\frac{2}{3}$ vacancy jog line and the dissociated dislocation along DC (Fig. 12(a)) and between the $\frac{1}{3}$ vacancy jog line and the dissociated dislocation along DB are illustrated in Figure 14(b). For the $\frac{2}{3}$ vacancy jog line we have,

$$\mathbf{B\alpha}+\boldsymbol{\alpha\delta} = \mathbf{B\delta}\,, \qquad \boldsymbol{\alpha}\mathbf{B}+\mathbf{B\delta} = \boldsymbol{\alpha\delta}\,,$$

and for the $\frac{1}{3}$ vacancy jog line,

$$\mathbf{B\alpha}+\boldsymbol{\alpha}\mathbf{C} = \boldsymbol{\beta}\mathbf{C}\,, \qquad \boldsymbol{\beta}\mathbf{C}+\mathbf{C\alpha} = \boldsymbol{\beta\alpha}\,.$$

The dislocation **CB** in Figure 14(b) is eliminated by the reactions

$$\mathbf{B}\boldsymbol{\delta}+\boldsymbol{\delta}\mathbf{A} = \mathbf{BA}\,, \qquad \mathbf{CB}+\mathbf{BA} = \mathbf{CA}\,,$$

$$\mathbf{A}\boldsymbol{\beta}+\boldsymbol{\beta}\mathbf{C} = \mathbf{AC}\,, \qquad \mathbf{CA}+\mathbf{AC} = 0\,.$$

Thus the original configuration of the dissociated Frank dislocation is returned. All other interactions between the climbed regions and between the climbed regions and the dissociated Frank dislocation are similar to those already discussed.

The final configuration of the loop after one unit of climb upwards in 1, 4, 2 and downwards in 5, 3, 6 (Fig. 12(a)) is one containing an unfaulted step on $(11\bar{1})$ bounded by the Shockley dislocations $\mathbf{B}\boldsymbol{\alpha}$ and $\boldsymbol{\alpha}\mathbf{B}$ along the step edges and the dislocations **AB** and **BA** along the step risers. The step may lower its energy by faulting; the reactions

$$\boldsymbol{\delta}\mathbf{B}+\mathbf{B}\boldsymbol{\alpha} = \boldsymbol{\delta}\boldsymbol{\alpha} \qquad \text{and} \qquad \mathbf{AB}+\mathbf{B}\boldsymbol{\delta} = \mathbf{A}\boldsymbol{\delta}$$

giving an intrinsically faulted step bounded by low energy stair-rod dislocations along the step edges and Shockley dislocations along the step risers.

Constriction of a dissociated Frank dislocation loop is not required for fault climb and thus a vacancy supersaturation can be reduced by this mechanism for a dissociated Frank dislocation loop when addition of vacancies at the edges of the loop would require constriction.

In deciding between the two models for the formation of stepped loops, the relatively high incidence of such loops should be considered. The formation of stepped loops by a combination of two Frank loops requires that dissociation is coplanar. This should be a relatively rare event, particularly in view of the low density of loops involved in the present experiments. Such an objection, however, does not apply to the climb model. Further, if dissociation resulting in the combination of two loops was the main mechanism for forming steps, a higher incidence of loops of the form shown in Figure 3(c) would be expected. However, the observation in Figure 3(c) suggests that combination of two Frank loops can occur and it is likely that a small proportion of complex loops may result in this way.

Only two types of Burgers vector for the dislocations at the step edge have been identified in these experiments: $\frac{1}{6}\langle 110\rangle$ corresponding to faulted steps, and $\frac{1}{6}\langle 112\rangle$ corresponding to unfaulted steps. The $\frac{1}{6}\langle 110\rangle$ Burgers vector is the only reasonable possibility for steps formed by the union of two loops and for the climb model this Burgers vector is the most likely. Unfaulted obtuse steps bordered by dislocations with $\frac{1}{6}\langle 112\rangle$ Burgers vectors could not arise by the union of two loops, but could arise by climb if the climbed region departs from a triangular configuration, so that its edges consist of $\frac{1}{3}$ and $\frac{2}{3}$ vacancy jog lines. Whilst the $\frac{2}{3}$ vacancy jog line seems unlikely, since it is readily converted by allowable shears to a $\frac{1}{3}$ vacancy jog line, the observations of the $\frac{1}{6}\langle 112\rangle$ Burgers vectors suggest that the $\frac{2}{3}$ vacancy jog line has been stabilized. Such steps would not be expected to fault as faulting would involve formation of high energy stair-rod dislocations of the $\frac{1}{6}\langle 310\rangle$ type.

The configuration of the loop in Figure 5 could not arise by the union of two separate loops and the alternatives in this case are that the defect consists of overlapping Frank loops or has resulted from fault climb. The presence of a triangular region within the hexagonal loop is similar in appearance to the double loops observed in aluminium, except that in this case one edge of the triangular region is coincident with an edge of the hexagon. As shown in Section V, the contrast at the edges of the triangular region is incompatible with overlapping Frank loops and shows that the two edges within the hexagonal loop are faulted steps bordered by $\frac{1}{6}\langle 110\rangle$ stair-rod dislocations. This configuration could only have arisen by fault climb.

The regular forms of complex loops in Figures 5 and 8 are common and can result from climb up and climb down, as discussed above. For example, nucleation of climb in regions 1, 2, 5, and 6 of Figure 12(*a*) would lead to climb up in 1 and 2 and climb down in 5 and 6 and further addition of vacancies to the fault would unite 1 and 2 and 5 and 6. The final stage would be the union of $\frac{2}{3}$ vacancy jog lines with the dissociated Frank along CD and EF, giving one unit of climb upwards in region 1, 4, 2, and downwards in region 5, 3, 6. This would produce the regular configuration of Figure 8. Similarly, the triangular configuration of Figure 5 could arise by climb up in region 1 and down in 4, 5, and 6 (Fig. 12(*a*)). The absorption of further vacancies would unite 5 and 6 and 4 and 6 with the final stage being the union of $\frac{2}{3}$ vacancy jog lines with the dissociated Frank along BD and EF. Continuation of up and down climb processes would lead to changes in the shape of loops as the step height increased. This discussion in terms of a small number of climbed regions is probably over-simplified and it is likely that the observed loop configurations arise from the interaction of many regions of climb.

Since constriction of a dissociated Frank is not necessary for the absorption of vacancies by fault climb, this method of growing loops may be the operative one in materials of low stacking fault energy once the edges of the loops are sufficiently aligned along $\langle 110\rangle$ directions for dissociation to occur. The present experiments provide evidence for the theory of Escaig that fault climb can occur by the absorption of vacancies.

VIII. Acknowledgments

We are indebted to Dr. P. Humble for the use of his computer programme, which he developed to treat problems of the type considered here, and to him and Dr. A. K. Head for many helpful discussions. We are extremely grateful to Mr. E. G. Beckhouse for photographic work.

IX. References

Clarebrough, L. M., and Morton, A. J. (1969*a*).—*Aust. J. Phys.* **22**, 351.
Clarebrough, L. M., and Morton, A. J. (1969*b*).—*Aust. J. Phys.* **22**, 371.
Clarebrough, L. M., Segall, R. L., and Loretto, M. H. (1966).—*Phil. Mag.* **13**, 1285.
Edington, J. W., and West, D. R. (1966).—*Phil. Mag.* **14**, 603.
Escaig, B. (1963).—*Acta Met.* **11**, 595.
Friedel, J. (1955).—*Phil. Mag.* **42**, 809.
Hashimoto, H., Howie, A., and Whelan, M. J. (1962).—*Proc. R. Soc.* A **269**, 80.
Head, A. K. (1967).—*Aust. J. Phys.* **20**, 557.
Head, A. K., Loretto, M. H., and Humble, P. (1967).—*Phys. Status Solidi* **20**, 505.
Howie, A., and Whelan, M. J. (1961).—*Proc. R. Soc.* A **263**, 217.
Humble, P. (1968).—*Aust. J. Phys.* **21**, 325.
Schapink, F. W., and de Jong, M. (1964).—*Acta Met.* **12**, 756.
Thompson, N. (1953).—*Proc. phys. Soc.* B **66**, 481.
Thompson, N. (1955).—Proc. Conf. on Defects in Crystalline Solids, London. p. 153.
Tunstall, W. J., and Goodhew, P. J. (1966).—*Phil. Mag.* **13**, 1259.